Anomalous microphotoluminescence of high-aspect-ratio Si nanopillars formatted by dry-etching Si substrate with self-aggregated Ni nanodot mask

Gong-Ru Lin[a)]
Graduate Institute of Electro-Optical Engineering and Department of Electrical Engineering, National Taiwan University, No. 1, Roosevelt Road, Sec. 4, Taipei 106, Taiwan, Republic of China

Chun-Jung Lin, Hao-Chung Kuo, Huang-Sheng Lin, and Chi-Chiang Kao
Department of Photonics, National Chiao Tung University, No. 1001, Ta Hsueh Road, Hsinchu 300, Taiwan, Republic of China and Institute of Electro-Optical Engineering, National Chiao Tung University, No. 1001, Ta Hsueh Road, Hsinchu 300, Taiwan, Republic of China

Microphotoluminescence (μ-PL) of high-aspect-ratio Si nanopillars fabricated by etching Ni-nanodot/SiO$_2$ masked Si substrate is investigated. The 320-nm-tall Si nanopillars obtained by CF$_4$/Ar mixed inductively coupled-plasma reactive ion etching process with density of 2.8×10^{10} cm^{-2} further shrink size from 30 to 6 nm by oxidation and etching. Blue-green μ-PL with two decomposed wavelengths at 425 and 475 nm is attributed to oxygen-related defects on the oxidized Si nanopillar surface. Defect-related near-infrared PL at 703 and 740 nm remains unchanged, while a quantum-confinement-effect-dependent PL blueshifted from 874 to 826 nm as the Si nanopillar size reduces from 7.2 to 6.0 nm is preliminarily observed. © *2007 American Institute of Physics.* [DOI: 10.1063/1.2719152]

The increasing interest in low dimensional Si structures has extended over the past decade due to their potential optoelectronic applications such as being nanoprobe,[1] surrounding gate or superjunction bipolar transistors,[2] memory cell,[3] biosensor,[4] photonic crystal waveguide devices,[5] field electron emitter,[6] and field emission light emitting devices.[7] Typically, the fabrication of Si nanopillars mainly relies on the electron-beam (E-beam) lithography and inductively coupled-plasma reactive ion etching (ICP-RIE) process.[8–10] The <10 nm Si nanopillar array can be produced under the assistance of E-beam lithography.[11] Nowadays, the self-assembled metallic nanodots have emerged to produce functional nanosensor or nanomask. Ni has been considered as an alternative to the noble metal (Au or Ag) for fabricating high-aspect-ratio Si nanopillars. Nevertheless, the self-aggregation of Ni nanodot from a Ni film coated on a Si substrate usually takes up to 10 min, and the generated Si nanopillars are too sparse.[12] In this letter, we demonstrate the formation of dense Si nanopillar array by reactive-ion-etching the oxide-covered Si substrate encapsulated with the self-assembled Ni nanodot mask. Anomalous microphotoluminescence (μ-PL) spectra of Si nanopillars at visible and near-infrared (NIR) spectral regions are also investigated.

A silicon dioxide (SiO$_2$) buffered layer with a thickness of 200 Å is deposited by plasma enhanced chemical vapor deposition under a standard recipe. A 50-nm-thick Ni film is evaporated on the SiO$_2$/Si substrate using an E-beam evaporator with a Ni deposition rate of 0.1 Å/s. Subsequently, the rapid thermal annealing (RTA) process at 850 °C for 22 s under the N$_2$ flowing gas of 5 SCCM (SCCM denotes cubic centimeter per minute at STP) is performed to assemble Ni nanodot patterns on the SiO$_2$/Si substrate, which is employed as an etching mask to dry-etch the Si substrate in an

ICP-RIE system (SAMCO ICP-RIE 101iPH) at rf of 13.56 MHz with different ICP/bias as power ratios. An etching gas mixture of CF$_4$ and Ar with a pressure ratio of CF$_4$/Ar=40 SCCM/40 SCCM was introduced to etch SiO$_2$/Si and to increase the vertical-etching potential, respectively. The dimension and density of the Si nanopillar array were analyzed by the scanning electron microscope (SEM) (Hitachi FE-SEM S-5000). Room-temperature μ-PL was performed in a confocal microscope with 1 μm spatial resolution by using a 325 nm HeCd laser and a 532 nm second-harmonic-generated (SHG) Nd:YAG (yttrium aluminum garnet) laser as the pumping sources. A 15× objective lens of numerical aperture 0.32 is used to collect the on-axis PL from the sample, which was received by a monochromator with a photomultiplying tube.

The SiO$_2$/Si substrate exhibits an extremely low thermal conductivity to facilitate heat accumulation of the evaporated thin Ni film and to enhance self-aggregation of the Ni nanodot array during RTA.[13] To assist the self-assembly of metallic nanodots, phase deformation, thermal vibration amplitude, and the melting point of metal atoms can apparently be detuned by thinning the deposited metal layer.[14] As a result, the density of the hemispherelike Ni nanodots with <40 nm diameter increases up to 7.2×10^{10} cm^{-2} at an optimized Ni film thickness of 50 Å (see Fig. 1). Lengthening the RTA duration could further shrink the nanodot size at a cost of reduced density. Low-pressure ICP-RIE was subsequently employed for obtaining high-aspect-ratio Si nanopillars with the Ni nanodot mask, as high-pressure condition enlarges the etching rate at a risk of overetching Ni nanodots and deforming Si nanopillars. Furthermore, the shape and aspect ratio of the Si nanopillars are significantly improved by decreasing the rf/bias power ratio, whereas the long-term enhanced isotropic etching at large rf/bias power ratio further erodes the Si nanopillars. A minor difference between vertical and horizontal etching rates inevitably provides a pyramidlike shape

---
[a)]Author to whom correspondence should be addressed; electronic mail: grlin@ntu.edu.tw
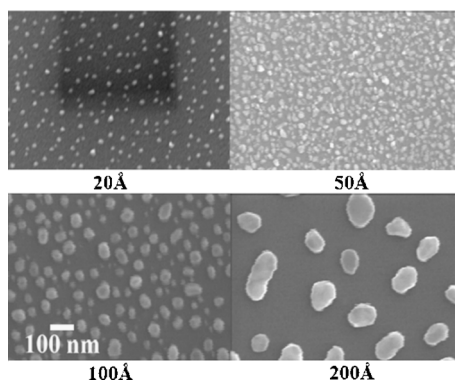
FIG. 1. (Color online) SEM image of Ni nanodots precipitated from the evaporated Ni film on SiO_2/Si with different film thicknesses.

FIG. 3. Density and average diameter of Si nanopillars on the Si substrate as a function of rf/bias power ratio in the ICP-RIE system.

of large size and reduced height. The rf/bias power ratio is thus decreased from 3 to 0.5 for obtaining straight Si nanopillars with perpendicular sidewall and high aspect ratio (see Fig. 2). The density, diameter, height, and corresponding aspect ratio of Si nanopillars are 2.8×10^{11} cm^{-2}, 30–44 nm, 320 nm, and up to 8, respectively [see Fig. 2(d)]. These results are relatively comparable with the reported aspect ratios between 7 and 12.[11,15] In contrast, a straight but short Si nanopillar shown in Fig. 2(c) was formatted at the rf/bias power ratio of 1, while an extremely large vertical-etching rate leads to the extinguishment on selective etching between Ni nanodot mask and Si substrate during ICP-RIE. The SEM illustrated in Fig. 3 reveals a significant variation on diameter and density of Si nanopillars formatted under different rf/bias power ratios. ICP-RIE at higher rf and bias powers at a constant ratio may contribute to uniform but smaller Si nanopillars due to insufficient etching rate.

A peak μ-PL at around 430 nm is observed after removing Ni and SiO_2 nanodots on top of Si nanopillars [see Fig. 4(a)], in which two decomposed luminescent centers at 425 and 475 nm are obtained with their spectral linewidths of 60 and 110 nm, respectively, corresponding to oxygen-related structural defects on the surface of Si nanopillars, such as weak oxygen bond, O_2^- defect center, neutral oxygen vacancy, and nonbridge oxygen hole center (NBOHC) at 415, 430, 455, and 630 nm, respectively.[16–21] Such intense blue PL emissions were preliminarily found in the electrochemically etched porous Si (PS) structures after rapid thermal oxidation,[22] providing a strong evidence on the influence of oxygen-related defects within surface SiO_2 due to a strong
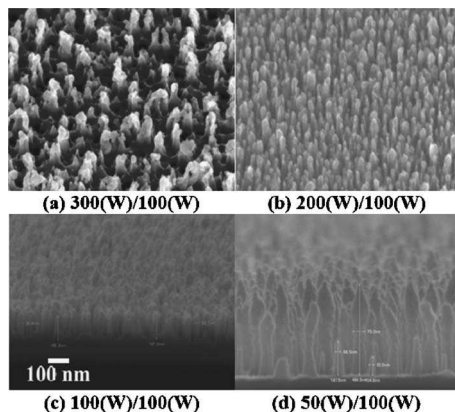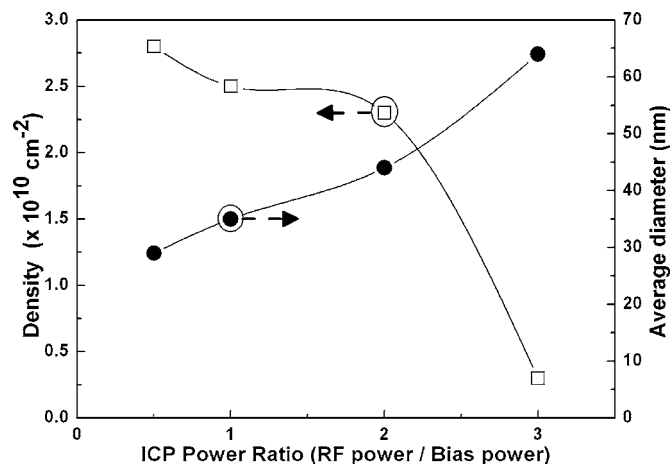
correlation between the observed blue PL and the Si–O infrared absorption. Ito *et al.*[23] and Chen *et al.*[24] have also corroborated the effect of the highly oxidized PS surface on the broadened 430 nm PL peak. The oxygen atoms would be incorporated in SiH_x backbones as ambient oxidation proceeds; a SiO_2 film naturally grows upon the surface of Si nanopillars with a maximum oxygen penetrating depth of 3 nm. Such a SiO_2 based PL model is widely accepted to corroborate that the blue PL from Si nanopillars is correlated with oxygen-related defects in naturally formed SiO_2 on a Si nanopillar in an atmospheric environment.

Later on, the Si nanopillar-related infrared PL excited by a SHG Nd:YAG laser at 532 nm was characterized. Note that both the Si nanopillars and the unprocessed Si wafer reveal the same PL signal around 700–750 nm with two distinct peak wavelengths at 703 and 740 nm [see Fig. 4(b)]. All Si nanopillar samples with different sizes were characterized to confirm the invariability of the 750-nm PL, which is not directly correlated with the Si nanopillar structure but can be attributed to other irradiative defects in the Si matrix. To perform such an analysis, the size of Si nanopillar samples at 30–50 nm was reduced by successive natural oxidation in an atmospheric environment and by chemical etching in buffer-oxide-etching solution. A plan-view SEM picture shows that

(a) 300(W)/100(W)   (b) 200(W)/100(W)
(c) 100(W)/100(W)   (d) 50(W)/100(W)

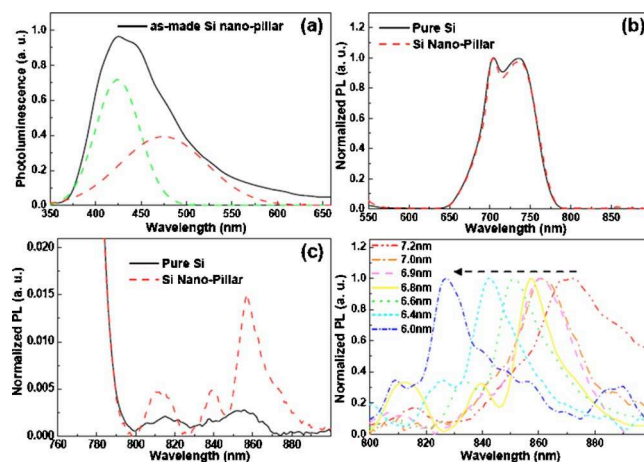FIG. 2. SEM image of Si nanopillars formed after ICP-RIE with different rf/bias power recipes.

FIG. 4. (Color online) (a) Micro-PL spectrum of as-made Si nanopillar array. (b) Normalized PL spectra of unprocessed pure Si wafer and etched Si nanopillar. (c) Si nanopillar-related PL and pure Si PL specta. (d) PL spectra of etched Si nanopillars.
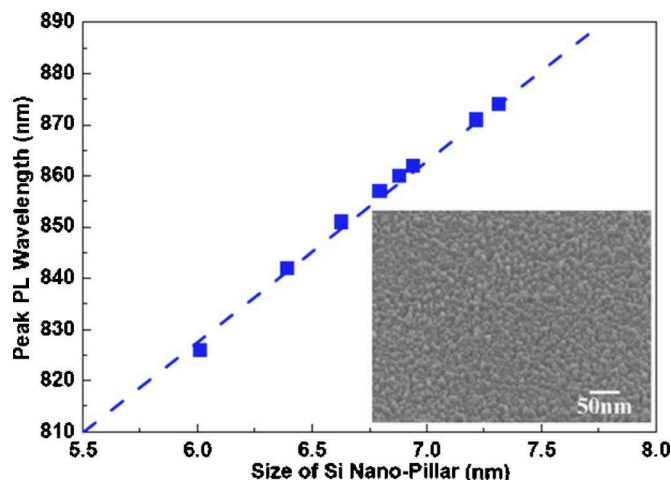
FIG. 5. (Color online) Peak wavelength of Si nanopillars as a function of rod size. Inset: Plan-view SEM picture of etched Si nanopillars.

the smallest size of the obtained Si nanopillar is about 6 nm (see the inset of Fig. 5). The PL of all Si nanopillar samples was taken immediately after oxidation and etching. Experimental results preliminarily elucidate that neither the SiO_2 nor the Si nanopillar can contribute to 750 nm PL since the SiO_2 film on the Si nanopillar surface was completely removed.

In contrast to the significant PL spectrum at 700–750 nm, a tiny PL between 800 and 900 nm was also observed from the sample with a Si nanopillar size smaller than 7.2 nm [see Fig. 4(c)]. The relatively small PL intensity is primarily due to the insufficient density of the Si nanopillars (only with a surface density of $2.8 \times 10^{10}/cm^2$). A blueshifted PL phenomenon with its wavelength decreasing from 874 to 826 nm was clearly observed as the Si nanopillar size shrinks from 7.2 to 6 nm [see Fig. 4(d)]. The SEM observed Si nanopillar size correlates well the theoretical value of $\lambda = 1.24/(1.12 + 3.73/d^{1.39})$, as reported by Delerue, *et al.*[25] which estimates the rod size of the etched Si nanopillars ranging from 7 to 5.7 nm according to their corresponding PL wavelengths. The broadened linewidth of PL from the Si nanopillar sample was shrunk from 50 to 17 nm due to the formation of the Si quantum pillar. As the Si nanopillar size becomes larger than 7.2 nm, the PL gradually decreases due to diminishing quantum-confinement effect (QCE). It is concluded that the size dependent PL can only be observed when the size of Si enters the quantum-confined regime, which is directly attributed to the recombination of quantum-confined electron and hole pairs in the Si nanopillars. Prior to the successive oxidation and etching, the Si nanopillar with average size of >30 nm and height of 320 nm is unavailable to contribute any QCE related luminescence, except the defect dependent PL remaining unchanged at 700–750 nm. The evolution of the peak PL wavelength for different etched Si nanopillars as a function of size is shown in Fig. 5.

In summary, anomalous μ-PL characteristics of dense Si nanopillars fabricated by dry-etching a SiO_2 covered Si substrate with a Ni nanodot mask is investigated. The optimum

ICP-RIE recipes for Si nanopillars with the highest density and aspect ratio are under a chamber pressure of 0.66 Pa and a rf/bias power ratio of 0.5. After ICP-RIE for 5 min, the obtained density, diameter, and height of the Si nanopillars are up to 2.8×10^{10} cm^{-2}, 30 nm, and 320 nm, respectively. Both the visible and NIR PLs from the high-aspect-ratio Si nanopillars were observed. The blue-green PL at around 430 nm is mainly attributed to oxygen-related defects formed on the surface of the Si nanopillars. The defect-related NIR PL at 703 and 740 nm from the Si substrate remain unchanged before and after formatting Si nanopillars, while a blueshifted PL phenomenon with its wavelength decreasing from 874 to 826 nm is clearly observed as the Si nanopillar size shrinks from 7.2 to 6 nm. Such a rod-size-dependent PL preliminarily confirms the occurrence of QCE on Si nanopillars at diameters <7 nm.

[1] T. Arai and M. Tomitori, Appl. Phys. Lett. **86**, 073110 (2005).
[2] F. D. Bauer, Solid-State Electron. **48**, 705 (2004).
[3] H. Pein and J. D. Plummer, IEEE Electron Device Lett. **14**, 415 (1993).
[4] Y.-K. Choi, J. S. Lee, J. Zhu, G. A. Somorjai, L. P. Lee, and J. Bokor, J. Vac. Sci. Technol. B **21**, 2951 (2003).
[5] V. Poborchii, T. Tada, and T. Kanayama, Opt. Commun. **210**, 285 (2002).
[6] M. Terauchi, N. Shigyo, A. Nitayama, and F. Horiguchi, IEEE Trans. Electron Devices **44**, 2303 (1997).
[7] M. J. Colgan and M. J. Brett, Thin Solid Films **389**, 1 (2001).
[8] M. Francois, J. Danlot, B. Grimbert, P. Mounaix, M. Muller, O. Vanbesien, and D. Lippens, Microelectron. Eng. **61**, 537 (2002).
[9] P. B. Fischer, K. Dai, E. Chen, and S. Y. Chou, J. Vac. Sci. Technol. B **11**, 2524 (1993).
[10] G. Nassiopoulos, S. Grigoropoulous, D. Papadimitriou, and E. Gogolides, Appl. Phys. Lett. **66**, 1114 (1995).
[11] J. S. Lee, S. K. Kim, G. Y. Yeom, J. B. Yoo, and C. Y. Park, Thin Solid Films **475**, 41 (2005).
[12] H. W. Huang, C. C. Kao, T. H. Hsueh, C. C. Yu, C. F. Lin, J. T. Chu, H.-C. Kuo, and S. C. Wang, Mater. Sci. Eng., B **113**, 125 (2004).
[13] G.-R. Lin, H.-C. Kuo, H.-S. Lin, and C. C. Kao, Appl. Phys. Lett. **89**, 073108 (2006).
[14] Q. Jiang, S. Zhang, and M. Zhao, Mater. Chem. Phys. **82**, 225 (2003).
[15] Y. Homma, P. Finnie, T. Ogino, H. Noda, and T. Urisu, J. Appl. Phys. **86**, 3083 (1999).
[16] P. Muttia, G. Ghislotti, S. Bertoni, L. Bonoldi, G. F. Cerofolini, L. Meda, E. Grilli, and M. Guzzi, Appl. Phys. Lett. **66**, 851 (1995).
[17] G.-R. Lin, C. J. Lin, and K. C. Yu, J. Appl. Phys. **96**, 3025 (2004).
[18] R. Tohmon, Y. Shimogaichi, H. Mizuno, Y. Ohki, K. Nagasawa, and Y. Hama, Phys. Rev. Lett. **62**, 1388 (1989).
[19] G.-R. Lin, C. J. Lin, C. K. Lin, L.-J. Chou, and Y. L. Chueh, J. Appl. Phys. **97**, 094306 (2005).
[20] H. Nishikawa, R. E. Stahlbush, and J. H. Stathis, Phys. Rev. B **60**, 15910 (1999).
[21] L. Skuja, J. Non-Cryst. Solids **239**, 16 (1998).
[22] G. Amato, C. Delerue, and H. J. Von Bardeleben, *Structural and Optical Properties of PS Nanostructures* (Gordon and Breach, Amsterdam, 1997), Vol. 5, p. 42.
[23] T. Ito, T. Ohta, and A. Hiraki, Jpn. J. Appl. Phys., Part 2 **31**, L1 (1992).
[24] Q. W. Chen, X.-J. Li, G. E. Zhou, J. S. Zhu, S. Y. Zhang, Y. B. Jia, and Y. H. Zhang, J. Appl. Phys. **81**, 7970 (1997).
[25] C. Delerue, G. Allan, and M. Lannoo, Phys. Rev. B **48**, 11024 (1993).